Supporting information for article

PROTON-DETECTED FAST-MAGIC-ANGLE SPINNING NMR OF PARAMAGNETIC INORGANIC SOLIDS

Jan Blahut[1]
Ladislav Benda[1]
Arthur L. Lejeune[1,2]
Kevin J. Sanders[1]
Benjamin Burcher[2]
Erwann Jeanneau[3]
David Proriol[2]
Leonor Catita[2]
Pierre-Alain R. Breuil[2]
Anne-Agathe Quoineaud[2]
Andrew J. Pell[1,4]
Guido Pintacuda*[,1]

[1] *Université de Lyon, Centre de RMN à Très Hauts Champs de Lyon (UMR 5082 - CNRS, ENS Lyon, UCB Lyon 1), 5 rue de la Doua, 69100 Villeurbanne, France*
[2] *IFP Energies Nouvelles, Rond-point de l'échangeur de Solaize, 69360 Solaize, France*
[3] *Université de Lyon, Centre de Diffractométrie Henri Longchambon (UCB Lyon 1), 5 rue de la Doua, 69100 Villeurbanne, France*
[4] *Stockholm University, Department of Materials and Environmental Chemistry, Svante Arrhenius väg 16C, SE-106 91 Stockholm, Sweden*

Contents

1. Sample preparation

General Considerations

Unless stated otherwise, all reactions were carried out under an atmosphere of argon using standard Schlenk techniques. Solvents were purified and degassed by using standard procedures. All reagents were purchased from commercial suppliers and used without further purification. FT-IR spectra were recorded in the solid state by an ATR Golden Gate (Specac) on a PerkinElmer spectrum one spectrometer. Elemental analyses were determined at London Metropolitan University.

Synthesis of $FeCl_2(THF)_{1.5}$

Anhydrous $FeCl_2$ (5 g) was placed into a Soxhlet paper cartridge. A round bottom flask was charged with THF (150 mL) prior to be connected to the Soxhlet apparatus under argon. After 3 days of reflux a suspension of a white solid in a brown solution was obtained. The solid was filtered and washed with THF (30 mL) and dried under reduced pressure giving 6.77 g (73 %) of a white powder. Anal. found (calcd.) for $FeCl_2$•$1.5C_4H_8O$: C, 30.6 (30.7); H, 4.99 (5.15). IR (solid): ν(C-O-C THF): 875, 1023 cm^{-1}.

Synthesis of the N-(diisopropylphosphino)-N-methylpyridin-2-amine (py-NMe-PiPr$_2$)

The synthesis of the ligand was performed following the procedure described by Gambarotta's group.[1] 2-methylaminopyridine (1.0 mL, 9.80 mmol, 1.00 eq.) was dissolved in diethylether (30 mL) and the solution was cooled to -78 °C. *n*-BuLi (6.30 mL, 10.1 mmol, 1.03 eq.) was added dropwise to yield a light yellow solution which was then stirred for 1 h at -78 °C and for 2 h at ambient temperature. Diisopropylchlorophosphine (1.6 mL, 10.1 mmol, 1.03 eq.) was then added dropwise at 0 °C, and the reaction mixture was stirred overnight. The white suspension was transferred on an alumina column and washed with diethylether. The solvent was evaporated under reduced pressure until precipitation occurred. The product was filtered on paper disc and evaporated to dryness offering 1.90 g (86 %) of a colourless oil.

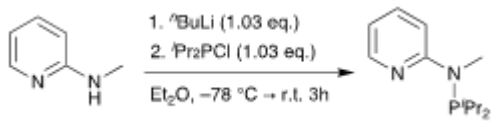

Scheme S1. Synthesis of the py-NMe-P*i*Pr$_2$ ligand.

Synthesis of the $FeCl_2$[py-NMe-PiPr$_2$)]

The py-NMe-P*i*Pr$_2$ ligand (0.674 g, 3.01 mmol, 1.05 eq.) and $FeCl_2(THF)_{1.5}$ (0.674 g, 2.87 mmol, 1.00 eq.) were suspended in toluene (20 mL) and stirred for two days at room temperature. A white solid precipitate was formed, which was subsequently filtered, washed twice with diethylether (30 mL) and dried under reduced pressure giving 0.917 g (91 %) of a white solid.

2. Sample characterization

The composition of the bulk was confirmed by elemental analysis. Anal. found (calcd.) for $C_{13}H_{22}Cl_2FeNP$: C, 41.05 (41.1), H, 6.12 (6.03), N, 7.82 (7.98).

Single crystals suitable for X-ray diffraction were obtained by vapor diffusion of pentane into a concentrated dichloromethane/toluene solution of complex **1**. A crystal was selected and mounted on a nylon loop in perfluoroether oil on a Gemini kappa-geometry diffractometer (Rigaku Oxford Diffraction) equipped with an Atlas CCD detector and using Mo radiation (λ= 0.71073 Å). Intensities were collected at 150 K by means of the CrysalisPro software.[2] Reflection indexing, unit-cell parameters refinement, Lorentz-polarization correction, peak integration and background determination were carried out with the CrysalisPro software. [2] An analytical absorption correction was applied using the modeled faces of the crystal.[3] The resulting set of hkl was used for structure solution and refinement. The structures were solved with the ShelXT[4] structure solution program using the intrinsic phasing solution method and by using Olex2[5] as the graphical interface. The model was refined with version 2018/3 of ShelXL [6] using full matrix least squares minimization on $\boldsymbol{F^2}$. All non-hydrogen atoms were refined anisotropically. Hydrogen atom positions were calculated geometrically and refined using the riding model.

Crystal data	
Chemical formula	$C_{12}H_{21}Cl_2FeN_2P$
M_r	351.03
Crystal system, space group	Monoclinic, $P2_1/c$
Temperature (K)	293
a, b, c (Å)	12.3959 (11), 23.352 (2), 11.4368 (10)
β (°)	95.280 (7)
V (Å^3)	3296.6 (5)
Z	8
Radiation type	Mo $K\alpha$
μ (mm^{-1})	1.32
Crystal size (mm)	0.60 × 0.48 × 0.39
Data collection	
Diffractometer	Xcalibur, Atlas, Gemini ultra
Absorption correction	Analytical
T_{min}, T_{max}	0.569, 0.706
No. of measured, independent and observed [$I > 2\sigma(I)$] reflections	38663, 8368, 6789
R_{int}	0.090
$(\sin \theta/\lambda)_{max}$ (Å^{-1})	0.692
Refinement	
$R[F^2 > 2\sigma(F^2)]$, $wR(F^2)$, S	0.062, 0.170, 1.05
No. of reflections	8368
No. of parameters	335
H-atom treatment	riding
$\Delta\rho_{max}$, $\Delta\rho_{min}$ (e Å^{-3})	1.11, −0.95

Table S1. Single-crystal X-ray diffraction experimental details

CCDC 2063303 contains the supplementary crystallographic data for this paper. These data can be obtained free of charge from The Cambridge Crystallographic Data Centre via www.ccdc.cam.ac.uk/structures.

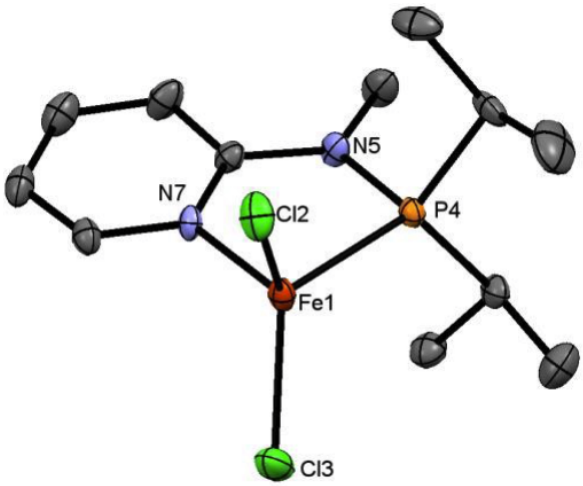

Figure S1. Thermal ellipsoid representation (at 50% probability) of complex **1**. Hydrogen atoms have been omitted for clarity. Selected bond lengths (Å) and angles (°): P4-Fe1-N7 80.00(9); Cl2-Fe1-Cl3 121.11(5); N7-Fe1 2.075(3); P4-Fe1 2.419(11); Cl2-Fe1 2.247(12); Cl3-Fe1 2.228(13).

3. Solid-state NMR

Temperature calibration and gradients.
The sample temperature inside the 1.3 mm rotor was calibrated using the changes in the ^{207}Pb chemical shift of $PbNO_3$, which depend linearly on the temperature with a slope of 0.753 ppm/°C, as published.[7] The ^{207}Pb chemical shift was set to 0 ppm for a static sample, for which the thermocouple readout indicated 0 °C. At 60 kHz MAS, frictional heating caused a temperature increase of +52 °C with respect to the thermocouple readout. Temperature gradients within the sample were estimated to be ±5 °C from the width of the ^{207}Pb signal under the experimental conditions (60 kHz MAS, 260 K readout temperature).

^{13}C direct-excitation spectra
For ^{13}C 1D spectra (Figure S4B) acquired in the 1.3 mm probe, the π/2 ^{13}C pulse lengths was 1.11 µs at 100 W, corresponding to RF field strengths of 226 kHz, at offsets of 400 ppm. Spectra were acquired with a rotor-synchronized double adiabatic echo experiment with a total double-echo time of 66.68 µs at 60 kHz MAS (four rotor periods). The adiabatic refocusing pulses were 33.33 µs long and swept through 5 MHz with a RF field strength of 50 W. No heteronucler ^{1}H dipolar decoupling was applied during the experiment.

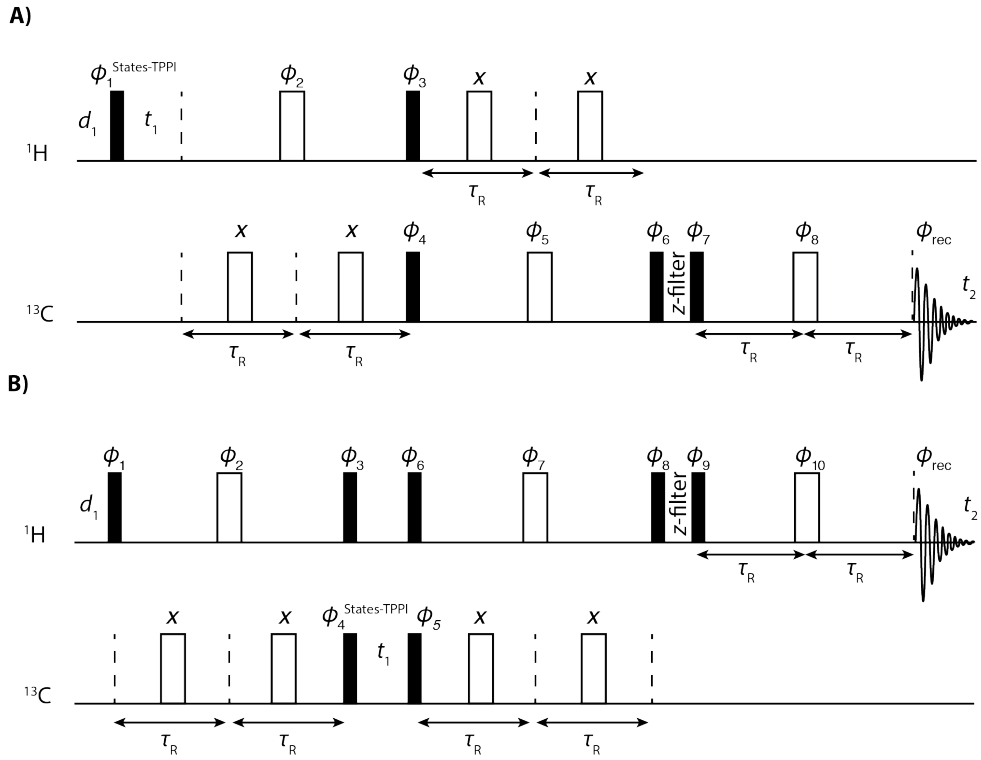

Figure S2. Pulse diagrams for A) ^{13}C-detected TEDOR and B) ^{1}H-detected HSQC-TEDOR. Black and empty rectangles indicate π/2 and π pulses respectively. The pulse phase was cycled as follows, where 0, 1, 2 and 3 indicate a x, y, -x and -y pulse phase respectively, and {*S* }**n* indicates the repetition of a given phase sequence for *n*-times*:* ϕ_1 = {0 2 1 3 2 0 3 1 2 0 3 1 0 2 1 3}; ϕ_2 = {1 3 2 0 3 1 0 2}; ϕ_3 = {1 1 2 2 3 3 0 0}; ϕ_4 = { 1 3 2 0 3 1 0 2}; ϕ_5 = {2 0 3 1 0 2 1 3}; ϕ_6 = {2 2 3 3 0 0 1 1}; ϕ_7 = {0 0 1 1 2 2 3 3 2 2 3 3 0 0 1 1}; ϕ_7 = {0 0 1 1 0 0 1 1}; ϕ_{rec} = {1 1 2 2 3 3 0 0} and **B)** ϕ_1 = {0 2}; ϕ_2 = {0 0 0 0 1 1 1 1}; ϕ_3 = ^{2}; ϕ_4 = {0 0 2 2}; ϕ_5 = {{0}*128 {2}*128}; ϕ_6 = ^{2}; ϕ_7 = {{0}*8 {2}*8}; ϕ_8 = ^{2}; ϕ_9 = {{1}*32 ^{2}*32 {3}*32 {2}*32}; ϕ_{10} = { {1}*16 {2}*16}; ϕ_{rec} = {0 2 2 0 2 0 0 2 2 0 0 2 0 2 2 0 2 0 0 2 0 2 2 0 0 2 2 0 2 0 0 2 1 3 3 1 3 1 1 3 3 1 1 3 1 3 3 1 3 1 1 3 1 3 3 1 1 3 3 1 3 1 1 3 2 0 0 2 0 2 2 0 0 2 2 0 2 0 0 2 0 2 2 0 2 0 0 2 2 0 0 2 0 2 2 0 3 1 1 3 1 3 3 1 1 3 3 1 3 1 1 3 1 3 3 1 3 1 1 3 3 1 1 3 1 3 3 1 2 0 0 2 0 2 2 0 0 2 2 0 2 0 0 2 0 2 2 0 2 0 0 2 2 0 0 2 0 2 2 0 3 1 1 3 1 3 3 1 1 3 3 1 3 1 1 3 1 3 3 1 3 1 1 3 3 1 1 3 1 3 3 1 0 2 2 0 2 0 0 2 2 0 0 2 0 2 2 0 2 0 0 2 0 2 2 0 0 2 2 0 2 0 0 2 2 0 2 0 0 2 1 3 3 1 3 1 1 3 3 1 1 3 1 3 3 1 3 1 1 3 1 3 3 1 1 3 3 1 3 1 1 3}. The pulse-phase with superscript $^{\text{States-TPPI}}$ are changed according the States-TPPI f_1 acquisition mode.[8] Short 50 µs and 100 µs z-filters were used in TEDOR and HSQC-TEDOR, respectively.

Due to the requirement of a rotor-synchronized sampling of the indirect dimension (f_1), the spectral width in the indirect ^{13}C dimension is limited by the MAS frequency. In the states-TPPI f_1 acquisition mode, this suppresses the spinning sidebands and removes line-shape distortions, [9] but also produces folding of signals resonating outside this spectral window. The position of the folded resonances was identified by recording a second HSQC-TEDOR spectrum at 58 kHz MAS, i.e., with a 58 kHz ^{13}C spectral widths in f_1. Between the two experiments, any signal folded *n*-times is shifted by $(n \times \Delta\text{SW})$ Hz in the indirect dimension, where $\Delta\text{SW} = 2$ kHz is the difference in spectral width between the two experiments. Here, a shift of 2 kHz and 4 kHz for the two C3 and C10 signals appearing respectively at $\delta(^1\text{H}) = 44$ and 265 ppm allowed to deduce the isotropic $\delta(^{13}\text{C})$ shifts of 570 and 1067 ppm, respectively, as illustrated in Figure S3.

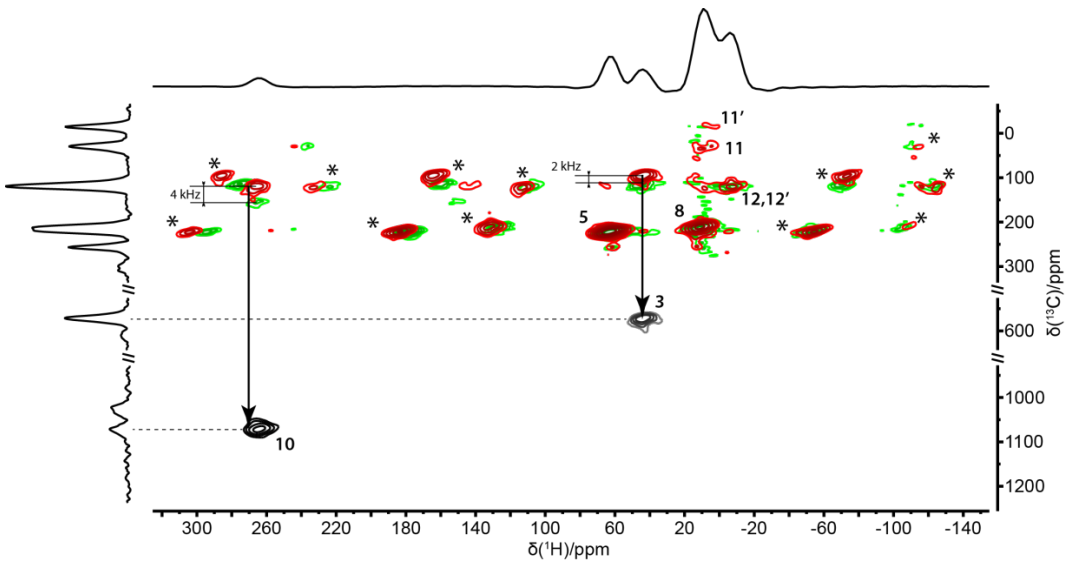

Figure S3. Piecewise measurement of the HSQC-TEDOR spectrum of complex **1** at 60 kHz MAS (315 K, 500 MHz). Overlapped are two ^{1}H-detected HSQC-TEDOR spectra acquired at 60 kHz MAS (^{13}C spectral width 60 kHz, red spectrum) and at 58 kHz MAS (^{13}C spectral width 58 kHz, green spectrum). The states-TPPI acquisition mode was used. In black, the reconstructed position of the C3 and C10 signals, unfolded from the red spectrum by 60 kHz and 120 kHz respectively. Asterisks (*) indicate ^{1}H rotational sidebands. On the sides of the horizontal and vertical axes are reported the ^{1}H aMAT isotropic projection and the directly-acquired ^{13}C MAS spectrum, respectively.

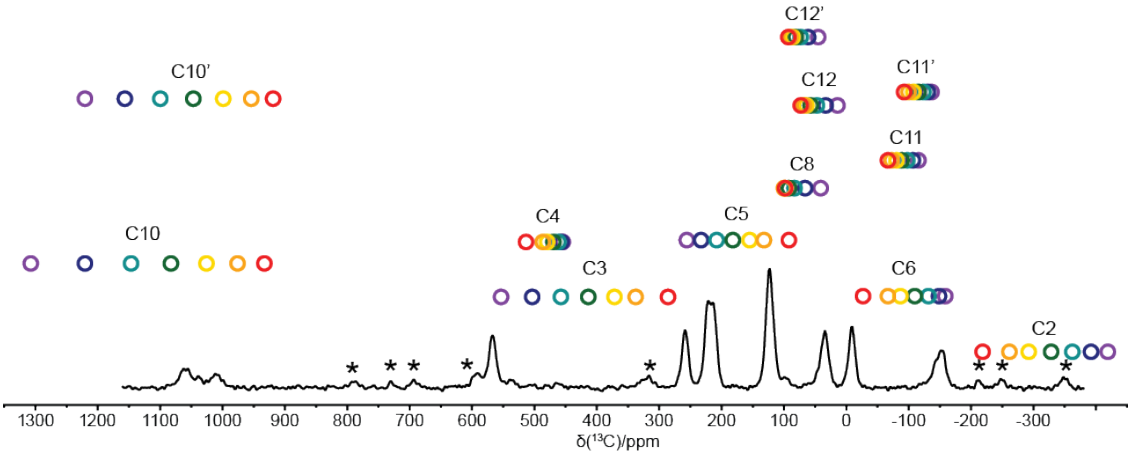

Figure S4. Solid-state ^{13}C NMR spectrum of **1** (312 K, 11.7 T, 60 kHz MAS). Rainbow-colored circles correspond to calculated shifts using different Hartree–Fock exchange admixtures to DFT functional used for hyperfine coupling calculations, ranging from 10 % (purple) to 40 % (red). For a complete list of predicted and experimental resonances, see Table S3.

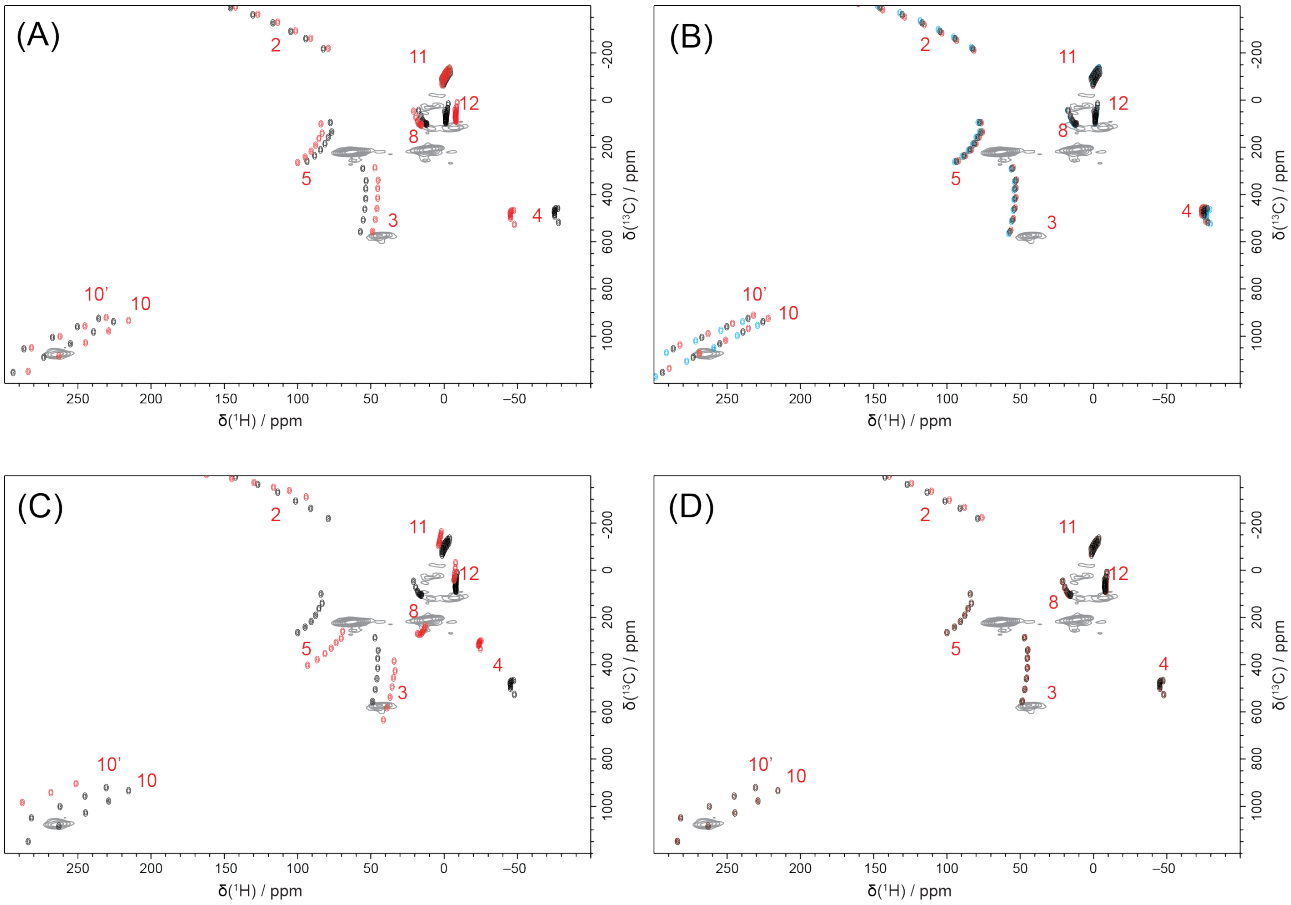

Figure S5. Assessment of secondary effects on the calculation of ^{1}H and ^{13}C shifts. Calculated shifts are overlaid onto the unfolded HSQC-TEDOR spectrum (grey). (A) Effect of intermolecular PCS: shifts were calculated with (black) and without (red) intermolecular PCS. Calculations were performed on the X-ray geometry with optimized hydrogen atoms, at a temperature of 312 K. (B) Effect of temperature: shifts were calculated at 307 K (blue), 312 K (black), 317 K (red) on the X-ray geometry with optimized hydrogen atoms. Intermolecular PCS were included in the calculations. (C) Effect of geometry optimization: shifts were calculated on the X-ray geometry with optimized hydrogen atoms (black) and on an *in-vacuo* fully-optimized structure (red; the molecule becomes C_s symmetric). Calculations were carried out at 312 K and did not include intermolecular PCS. (D) Effect of higher-order hyperfine coupling terms ("A2 terms"): shifts were calculated without (black) and with (red) the "A2 terms". Calculations were carried out on the X-ray geometry with optimized hydrogen atoms at a temperature of 312 K, and intermolecular PCS were not included.

4. Quantum chemistry calculations

Fe	5.9244853	14.0415541	8.0250597
Cl	4.3837298	15.5519606	7.3982459
Cl	5.3781045	11.9064807	8.3493007
P	7.5458189	14.9371028	9.5810303
N	8.8541175	15.1547427	8.5171806
C	8.7155086	14.8322518	7.1725430
N	7.5656349	14.2267350	6.7688091
C	7.4546869	13.8213441	5.4686505
C	8.4214566	14.0088611	4.5425727
C	9.5797513	14.6930739	4.9497276
C	9.7208363	15.1110748	6.2612912
H	10.6225242	15.6388603	6.5661951
H	10.3764774	14.9008546	4.2314633
H	8.2933997	13.6617791	3.5172398

H	6.5071815	13.3295781	5.2322632
C	10.1569851	15.6621816	9.0132945
H	10.3845742	16.6604446	8.6058528
H	10.1105502	15.7416397	10.1050158
H	10.9719056	14.9703039	8.7508439
C	8.2465747	13.8423611	10.9042269
C	7.1630720	13.3620102	11.8496937
H	7.5960060	12.6678570	12.5867344
H	6.6852870	14.1768356	12.4093690
H	6.3795252	12.8201542	11.2958271
C	8.9315625	12.6488404	10.2484451
H	9.3244392	11.9740504	11.0244001
H	9.7691152	12.9397060	9.5989121
H	8.2085909	12.0787227	9.6416529
H	8.9888840	14.4329418	11.4726272
C	7.3108249	16.6170453	10.2895031
C	7.2060060	17.6237491	9.1227814
H	7.0060338	18.6289453	9.5239670
H	8.1265490	17.6728346	8.5243860
H	6.3720258	17.3480813	8.4566162
C	6.0402583	16.6826643	11.1174989
H	5.8814567	17.7129065	11.4715471
H	6.0638706	16.0332401	12.0028394
H	5.1690204	16.3998830	10.5053639
H	8.1847736	16.8615515	10.9201963

Table S2. Cartesian coordinates of the XRD structure of complex **1** with hydrogen atoms optimized with DFT (PBE0-D3(BJ) / def2-SVP, Fe: def2-TZVP).

5. Summary of experimental and calculated shifts

Table S3. Experimental NMR shift in solid state (δ_K^{ss}) as well as calculated values (δ_K) obtained with Hartree–Fock exchange admixture (HFX) for hyperfine coupling calculation ranging from 10 to 40 %. Intermolecular PCS are included in all calculations. All values are listed in ppm.

HFX	10 %	15 %	20 %	25 %	30 %	35 %	40 %	
K				δ_K				δ_K^{ss}
H2	162.9	145.9	130.7	117.0	104.8	94.6	82.6	N/A [a]
H3	57.3	55.4	54.3	53.7	53.7	53.4	55.7	44
H4	-77.3	-75.8	-75.0	-74.9	-75.3	-75.2	-77.8	N/A [a]
H5	93.7	88.5	84.5	81.5	79.2	76.9	77.8	63
H8	17.6	16.0	14.8	13.8	13.0	12.3	12.0	11
H10	346.3	318.4	294.2	273.3	255.1	239.3	225.7	N/A [a]
H11	-4.0	-2.9	-2.0	-1.2	-0.5	0.1	0.6	6 [b]
H12	-2.6	-2.2	-2.0	-1.7	-1.5	-1.4	-1.2	-6 [b]
H10'	365.1	335.3	309.4	286.8	267.3	250.3	235.8	264.6
H11'	-3.6	-2.3	-1.2	-0.3	0.5	1.2	1.8	6 [b]
H12'	-0.2	-0.5	-0.6	-0.7	-0.8	-0.8	-0.9	-6 [b]
C2	-420	-393	-363	-329	-293	-262	-219	N/A [a]
C3	554	504	458	414	372	338	286	570
C4	455	457	462	470	480	487	514	257
C5	256	233	208	182	155	132	92	220
C6	-159	-149	-132	-110	-87	-67	-27	-157
C8	41	66	83	92	98	100	98	210
C10	1309	1222	1148	1084	1027	977	934	1067
C11	-116	-107	-98	-89	-81	-73	-67	30
C12	14	33	47	57	64	68	73	119 [b]
C10'	1222	1158	1101	1048	1000	955	920	1019 [c]
C11'	-137	-131	-124	-116	-108	-100	-93	-14 [c]
C12'	45	61	73	81	86	90	93	119 [b]

[a] Signals were not observed due to a fast inter/intramolecular paramagnetic-induced relaxation. [b] Signals from near-equivalent atoms of *iso*-propyl groups were not resolved. [c] Near-equivalent atoms of *iso*-propyl groups experiencing non-symmetry due to crystal packing were resolved in a ^{13}C MAS experiment.

References

1. Y. Yang, J. Gurnham, B. Liu, R. Duchateau, S. Gambarotta and I. Korobkov, *Organometallics*, 2014, **33**, 5749-5757.
2. *CrysalisPro Software System 1.171.40.67a*, Rigaku Oxford Diffraction, Oxford, UK, 2019.
3. R. C. Clark and J. S. Reid, *Acta Crystallographica Section A Foundations of Crystallography*, 1995, **51**, 887-897.
4. G. M. Sheldrick, *Acta Crystallogr A Found Adv*, 2015, **71**, 3-8.
5. O. V. Dolomanov, L. J. Bourhis, R. J. Gildea, J. A. K. Howard and H. Puschmann, *J. Appl. Crystallogr.*, 2009, **42**, 339-341.
6. G. M. Sheldrick, *Acta Crystallogr C Struct Chem*, 2015, **71**, 3-8.
7. A. Bielecki and D. P. Burum, *Journal of Magnetic Resonance, Series A*, 1995, **116**, 215-220.
8. D. Marion, M. Ikura, R. Tschudin and A. Bax, *J. Magn. Reson.*, 1989, **85**, 393-399.
9. R. Tycko, D. P. Weliky and A. E. Berger, *J. Chem. Phys.* , 1996, **105**, 7915.